Nanoscale Morphological Changes during Hydrolytic Degradation and Erosion of a Bioresorbable Polymer

Alioscka Sousa,[†,§] Jaap Schut,[‡] Joachim Kohn,[‡] and Matthew Libera*[,†]

Department of Chemical, Biomedical, and Materials Engineering, Stevens Institute of Technology, Hoboken, New Jersey 07030, and New Jersey Center for Biomaterials, Rutgers University, Piscataway, New Jersey 08854

Received June 8, 2006; Revised Manuscript Received July 19, 2006

ABSTRACT: The rate and mechanism of hydrolytic degradation and erosion determine the utility and performance of bioresorbable polymers for tissue-engineering and drug-delivery applications. Nevertheless, changes in polymer morphology at the nanoscale caused by degradation and erosion, particularly those associated with the spatial distribution of water, are not well understood. We exploit recent imaging advances based on spatially resolved electron energy-loss spectroscopy (EELS) in the cryo-scanning transmission electron microscope to quantitatively map the morphological changes of a degrading and eroding random copolymer of DTE (desaminotyrosyl-tyrosine ethyl ester) and PEG (poly(ethylene glycol)). Weight-gain measurements indicate that this polymer contains 12 wt % water after 48 h of immersion in water at 20 °C. After immersion for 5 months, EELS shows that the average water content increases from 11.8 ± 0.8 to 14.9 ± 1.0 wt %, but 15 nm resolution compositional maps do not reveal any morphological changes. After immersion for 12 months, however, compositional mapping resolves a network of PEG-depleted regions with characteristic sizes of 50−100 nm. These PEG-depleted regions are enriched in water. They correspond to high-diffusivity paths through which PEG-rich fragments eroded. Exposure to water at 37 °C for 2 additional weeks leads to an even more developed network of channels about 100 nm in size. These findings suggest that the development of high-diffusivity pathways at nanolength scales plays a key role in the early stages of bioresorption in bulk-eroding polymers, and they demonstrate that electron energy-loss spectroscopy in the STEM is an effective new tool to quantitatively study the morphological changes associated with polymer hydration, degradation, and erosion at these fine length scales.

1. Introduction

Bioresorbable polymers are currently under investigation for possible use in a wide range of medical devices such as vascular grafts, drug-delivery vehicles, and tissue-engineering scaffolds.[1−4] When in contact with a physiological medium, these polymers undergo degradation and erosion.[5] Degradation reduces the polymer molecular weight, while erosion leads to mass loss as the fragments produced by degradation diffuse out of the polymer. To gain a fundamental understanding of the erosion process, bioresorbable polymers have been extensively characterized with respect to their mass-loss profile, changes in crystallinity, and formation of pores.[6−9] In addition, extensive use has been made of mathematical modeling.[10−14] However, as was recently pointed out by Burkersroda et al.,[15] erosion is a complex phenomenon that remains far from being satisfactorily understood.

Bioresorbable polymers can be classified as either surface eroding or bulk eroding.[5,15] The mass-loss profile of bulk-eroding polymers typically follows a pattern where there is an initial period of no significant mass loss followed by an abrupt onset of rapid mass loss.[7,12,16,17] Göpferich explained many of the important features of bulk-erosion behavior by constructing a percolation model.[12] According to this model, water-soluble degradation products are only able to leave the bulk of a polymer after enough degradation has taken place so that a percolated microstructure constituted by water and the water-soluble degradation products extends to the surface. Using this model, Göpferich predicted the onset of spontaneous erosion after a period of no mass loss.

Though the percolation model can satisfactorily explain the mass-loss profile of bulk-eroding polymers, it does not address in detail the specific morphological changes that occur to a polymer undergoing erosion. For example, if pores and channels are created, knowing the characteristic length scales and spatial distribution of these features is important because these dynamic morphological changes have a direct impact on the mechanical integrity of the biomaterial device and its transport properties. While many experimental approaches have been utilized to study the real-space morphology of eroding polymers,[18] a comprehensive characterization of their morphological evolution is challenging. Specifically, early morphological changes can occur at length scales well below the spatial resolution limit of many of the available experimental characterization methods. Furthermore, since many bioresorbable polymer systems are multicomponent systems—copolymers[4,18,19] and blends[20,21]—which are phase separated at nano and micro length scales, unambiguously identifying the different chemical phases comprising the multicomponent system and their respective roles in the erosion process becomes crucial to understanding the erosion process. Finally, water is an integral part of a bioresorbable polymer system, and water−polymer interactions need to be explicitly taken into account. Macroscopic methods can be used to measure the degree of water uptake, the kinetics of this uptake, and the state of the water within a hydrated bioresorbable polymer, but no experimental method has yet mapped the nanoscale spatial distribution of water within a bioresorbable polymer and related this to the underlying polymer morphology.

† Stevens Institute of Technology.
‡ Rutgers University.
§ Present address: Division of Bioengineering and Physical Sciences, National Institutes of Health, Bethesda, MD 20892.
* Corresponding author: tel +1-201-216-5259; fax +1-201-216-8306; e-mail mlibera@stevens.edu.

10.1021/ma061286g CCC: $33.50
Published on Web 09/15/2006

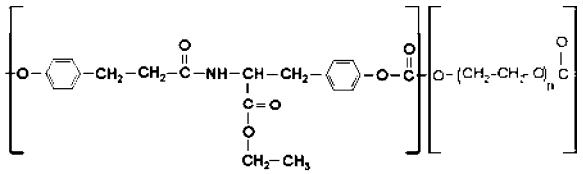

Figure 1. Structure of poly(DTE−PEG).

Here we describe research using spatially resolved electron energy-loss spectroscopy[22,23] (EELS) in the cryo-scanning transmission electron microscope (cryo-STEM) to study the morphological evolution and water distribution within a bulk-eroding bioresorbable copolymer system undergoing degradation and erosion. This approach combines the nanoscale spatial resolution of the scanning transmission electron microscope, the spectral sensitivity afforded by electron energy-loss spectroscopy, and the ability to work with frozen-hydrated specimens in the cryo-STEM to generate quantitative nanoscale compositional maps for water and for the phases comprising the multicomponent polymer system. In contrast to the TEM imaging of less radiation-sensitive materials where sub-angstrom resolution has recently been demonstrated and is limited by the quality of the microscope's optics,[24] the achievable resolution in studies of radiation-sensitive materials such as hydrated polymers is determined by the electron dose required to generate a statistically significant signal above noise.[25] The spatial resolution of 15 nm achieved in the present experiments is a factor of 5−10 better than previous studies of hydrated organics,[25−28] and it is a critical enabler of the experiments described here. These experiments permit us to quantitatively reveal nanoscale morphological changes associated with polymer hydration, degradation, and erosion.

We have studied a bulk-eroding, bioresorbable, random copolymer consisting of desaminotyrosyl-tyrosine ethyl ester (DTE) units copolymerized in random sequence with 8 mol % of low molecular weight PEG (1 kDa). This polymer belongs to a group of tyrosine-derived polycarbonates which are currently being considered for use in medical implant applications.[19,29] The polymer composition (Figure 1) can be represented by poly(DTE-*co*-8% PEG_{1000} carbonate)[19] and has been abbreviated here as p(DTE−PEG).

Degradation within p(DTE−PEG) occurs preferentially at the carbonate bond located in its backbone[30] (Figure 1). From such a degradation mechanism it is possible, for example, that an entire PEG segment is released from the copolymer chain provided that degradation takes place at both ends of the PEG oligomer. It is also possible that DTE without any PEG attached is formed. Since DTE is not readily water-soluble, this degradation reaction simply reduces the copolymer molecular weight. A degradation product consisting of both DTE and PEG can also be produced. Its solubility will depend on the balance of DTE and PEG. Furthermore, in addition to backbone carbonate bond cleavage there is also the possibility for cleavage of the pendent ester bond of the DTE (Figure 1). This produces the more water-soluble desaminotyrosyl-tyrosine (DT)[30] unit. The kinetics of this side-chain degradation mechanism are, however, ∼4 times slower than those of the main-chain carbonate bond cleavage.[30]

2. Experimental Section

2.1. Degradation Study. Poly(DTE-*co*-8% PEG carbonate) [p(DTE−PEG)] was synthesized as described previously.[19] For degradation studies, films about 300 μm thick were obtained by compression-molding. These films were placed in type I deionized water (18.2 Mohm·cm, pH 5.6) at 20 °C. At specific time points (2 days, 5 and 12 months), a piece of the copolymer was taken from the water and frozen in liquid nitrogen (2 days) or liquid propane (5 and 12 months).

2.2. Differential Scanning Calorimetry. Measurements were performed on a TA Instruments DSC 2920 under nitrogen. Prior to DSC analysis, specimens were equilibrated at room temperature and 50% relative humidity. The sample size and the scan rate were 8−15 mg and 10 °C/min, respectively. The glass transition was determined by the half-extrapolated tangents method from the second scan after a short annealing step 50 °C above T_g, followed by cooling at 10 °C/min.

2.3. TEM Specimen Preparation, HAADF STEM, and EELS. Frozen-hydrated films at each degradation time point were microtomed perpendicular to the plane of the film to generate cross sections. The microtomy was performed using a dry 35° diamond knife at −100 °C using a Leica Ultracut S cryo-ultramicrotome. The sections were placed on a Cu grid coated with a continuous layer of carbon (about 30 nm thick) and stored in liquid nitrogen. Specimens of pure amorphous ice were made by cryoplunging ultrathin water films supported by copper TEM grids into liquid propane, and specimens of pure PEG and PDTE were prepared by traditional cryomicrotomy of pure solid polymer specimens.

The imaging experiments used a Philips CM20 field-emission gun (FEG) scanning transmission electron microscope (TEM/STEM) at an accelerating voltage of 200 kV. This instrument is equipped with a Gatan (Pleasanton, CA) 776 Enfina magnetic prism electron energy-loss spectrometer and a Gatan Digiscan II control and acquisition system.

High-angle annular-dark-field (HAADF) STEM imaging was performed by scanning an electron beam with controlled diameter, interpixel spacing, and dwell time across 2 μm × 2 μm specimen areas. In this imaging mode, regions of the specimen with higher thickness or higher density preferentially scatter electrons to higher angles. These electrons are collected by a single-crystal YAG scintillator annular detector and give rise to bright pixels in the image. A focused electron beam with a dose per pixel of ∼100 e/nm^2 was used to acquire high-quality HAADF STEM images. During the selection of appropriate areas for EELS imaging, however, lower electron doses were used (less than 1 e/nm^2) in order to minimize specimen damage prior to the EELS data collection.

Electron energy-loss spectroscopic (EELS) imaging was performed by digitally rastering a 15 nm diameter electron probe with a 15 nm interpixel spacing across 2 μm × 2 μm specimen areas. The electron dose per pixel was ∼600 e/nm^2, and it was low enough to not cause significant damage to the specimen as manifested by changes in the EELS spectrum such as those brought by the evolution of molecular hydrogen.[25,31] From the spectra generated at each pixel of the data set, compositional maps of the components in the system were derived using the multiple-least-squares (MLS) approach. Detailed descriptions of the postacquisition processing and MLS analysis of low-loss energy-loss spectra are available in the literature.[25,32] Briefly, the shape of a properly postprocessed spectrum at a particular pixel position p_i depends on the fraction of water, PEG, and DTE in that same pixel. We determined the composition at the pixel p_i by fitting reference spectra characteristic of pure amorphous ice, homopolymer PEG, and homopolymer poly(DTE) (abbreviated as PDTE) (Figure 2) to the unknown experimental spectrum at p_i. Repeating the fitting procedure at each of the 15 nm wide pixels of the 2 μm × 2 μm area generates compositional maps (weight-fraction maps) for water, PEG, and DTE. For these calculations the total inelastic scattering cross sections per unit mass σ_m of the polymers and water were needed, and, following the method described by Sun et al.,[32] our measurements yielded for water, PEG, and PDTE σ_m of 3485 ± 50, 3977 ± 60, and 3770 ± 50 m^2/kg, respectively. By using pure reference spectra in the MLS analysis, we are making the assumptions that (1) secondary bonding between the three components does not significantly modify the spectral character of the three components and (2) hydrolytic degradation changes a small fraction of chemical bonds within the copolymer structure. The latter is certainly true

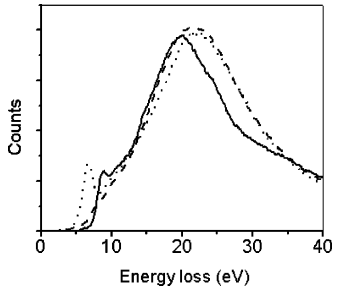

Figure 2. Low-loss electron energy-loss spectra characteristic of (—) amorphous ice, (- - -) PEG, and PDTE (•••).

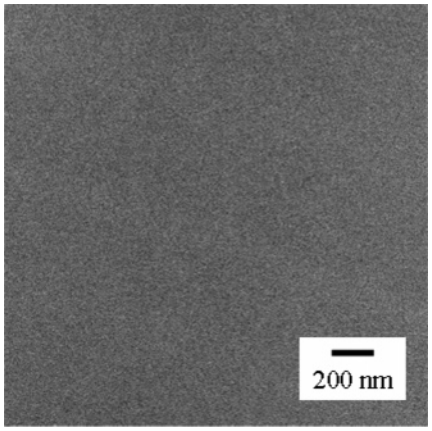

Figure 3. HAADF STEM image of a frozen-hydrated nondegraded p(DTE−PEG) film.

at the early stages of degradation and will become increasingly less true as degradation progresses. To confirm the reproducibility of our measurements, for each degradation time point (2 days, 5 and 12 months), we generated 10 maps from five different microtomed sections. Average values with corresponding standard errors of the mean for each of the degradation time points were derived from the 10 compositional maps.

3. Results and Discussion

First, we characterized a dry p(DTE−PEG) film in order to establish its initial morphology. DSC traces of pure PEG and pure PDTE indicated that the homopolymers have a dry T_g of −45 and 96 °C, respectively, while PEG additionally shows a melting point around 58 °C. The copolymer shows a major T_g at 41 °C and a small but reproducible second T_g at 86 °C, indicating microphase separation between PEG-rich domains and DTE-rich domains. Bright-field TEM imaging of a RuO_4-stained film[33,34] showed no contrast. From this we conclude that the PEG phase-separated domains are small (<5−10 nm in diameter) and randomly distributed so that in projection they overlap and cannot be distinguished from the DTE-rich major phase.

Next, we characterized the morphology of a nondegraded p(DTE−PEG) film that was immersed in water for 2 days. Time-resolved weight-gain measurements indicate that these films become saturated with water to a level of about 12 wt % after immersion for 2 days.[35] Figure 3 shows a high-angle annular dark-field (HAADF) STEM image of one such nondegraded frozen-hydrated p(DTE−PEG) film. This image has uniform contrast and agrees with our finding that phase-separated PEG domains must be small and aperiodically distributed throughout the DTE-rich matrix. To quantitatively characterize the initial spatial distribution of water and PEG within the nondegraded copolymer, we rastered a 15 nm diameter probe with a 15 nm interpixel spacing across a 2 μm × 2 μm region

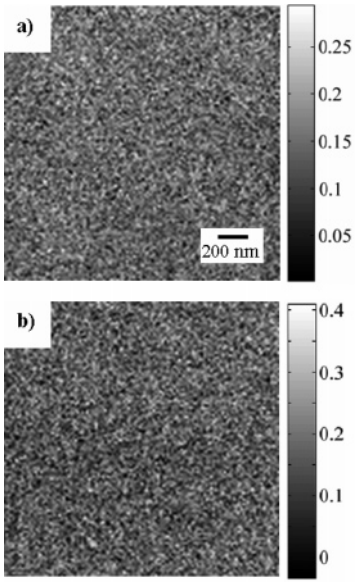

Figure 4. (a) Water and (b) PEG compositional maps from a nondegraded frozen-hydrated p(DTE−PEG) film. Pixel size = 15 nm. Numbers on gray scales correspond to weight fraction.

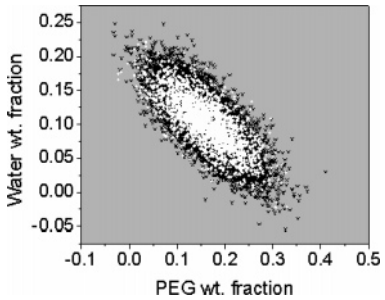

Figure 5. Water−PEG scatter diagram showing simulated noise cluster (white points) superimposed on experimental cluster (black points) generated from the compositional maps in Figure 4. The noise cluster is centered around a fixed composition, chosen as the average composition derived from the data set presented in Figure 4.

of the specimen. At each pixel position of this raster, low-loss EELS spectra were collected, and reference spectra characteristic of pure amorphous ice, PEG, and PDTE (Figure 2) were MLS fit to the experimental spectrum. Figure 4 shows the resulting 15 nm resolution quantitative weight-fraction water and PEG maps. From 10 such maps we obtained average water, PEG, and DTE weight percent values that agree well with the nominal composition of the specimen. Specifically, we measured 11.8 ± 0.7 wt % water, in good agreement with the average water content of ∼12 wt % determined by weight gain, and we measured a PEG-to-DTE ratio of 0.249 ± 0.015, also in good agreement with the PEG-to-DTE ratio in the dry copolymer of 0.232.

We then determined whether water and PEG are homogeneously distributed or show instead spatially varying compositional fluctuations. A direct inspection of Figure 4 reveals fluctuations at high spatial frequencies in both the water and PEG maps. These fluctuations could be noise intrinsically associated with our experimental procedure.[25] To differentiate between real fluctuations and noise, we constructed an experimental water−PEG scatter diagram over which we superimposed the intrinsic noise cluster associated with our set of experimental conditions (Figure 5). Details of how to construct and interpret these scatter diagrams are given elsewhere.[25] Since the noise cluster (white points in Figure 5) superimposes well over the experimental cluster (dark points in Figure 5), the great

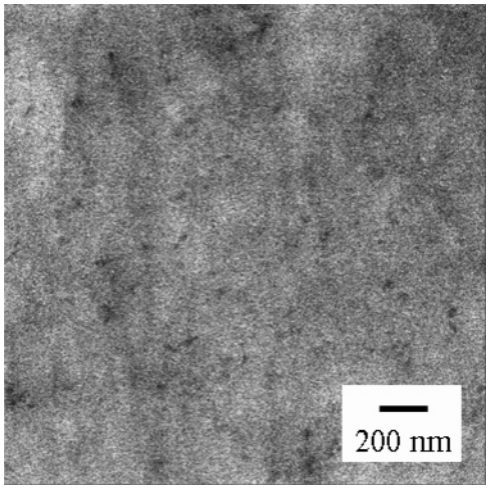

Figure 6. HAADF STEM image of a frozen-hydrated p(DTE−PEG) film after 12 months in water.

majority of fluctuations seen in the water and PEG maps are simply noise, and water and PEG can be considered homogeneously distributed at the spatial resolution of 15 nm. Because the water and PEG maps of the nondegraded copolymer are homogeneous at the resolution limit of these experiments, any changes to these maps from the analysis of degraded specimens can thus be directly associated with degradation and erosion of the copolymer.

Similar to Figure 3, an HAADF STEM image of a p(DTE−PEG) specimen after 5 months immersion in water at 20 °C does not reveal contrast indicative of significant morphological changes. Water and PEG maps also show contrast comparable to that in the maps presented in Figure 4 for the nondegraded case, and a scatter-diagram analysis confirmed that the compositions are indeed uniform. The PEG-to-DTE ratio after 5 months (0.232 ± 0.011) does not change significantly in relation to the nondegraded copolymer (0.249 ± 0.015). However, after 5 months the copolymer shows a slight increase in water content, going from the initial value of 11.8 ± 0.7 wt % to 14.9 ± 1.0 wt %.

Figure 6 shows an HAADF STEM image of the copolymer film after immersion of 12 months in water at 20 °C. Unlike the data collected from the earlier time points, we now clearly observe dark-contrast regions with characteristic diameters of ∼50−100 nm, suggesting that erosion occurs between the 5 and 12 month time points. However, HAADF STEM imaging does not allow us to unambiguously and quantitatively correlate the observed contrast features with changes in local specimen composition. We therefore created water and PEG compositional maps (Figure 7) using EELS in the STEM from a specimen region similar to the one displayed in Figure 6. The average of 10 different measurements shows that after 12 months of immersion the water content of the specimen increases from 11.8 ± 0.7 to 19.0 ± 1.2 wt %, and the PEG-to-DTE ratio decreases from 0.249 ± 0.015 to 0.184 ± 0.018, indicating that the loss of PEG-rich fragments occurred preferentially to that of DTE-rich fragments.

To characterize the possible changes associated with the spatial distribution of water and PEG arising from the preferential erosion of PEG-rich fragments, we consider the water and PEG maps shown in Figure 7 in conjunction with the scatter diagram of Figure 8. We believe the slight texture apparent in the maps is real. We do not observe such texture in all of the image data we collected, indicating that it is not a consequence of the cryo-microtomy specimen-preparation process. Figure 8

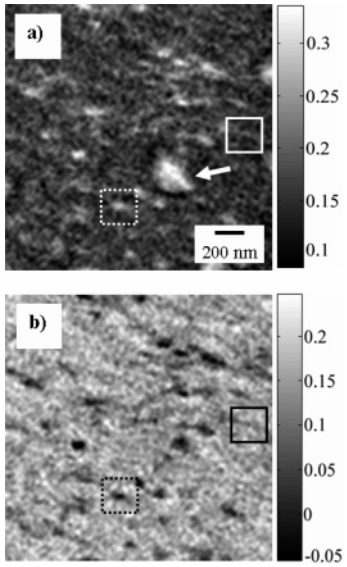

Figure 7. (a) Water and (b) PEG compositional maps from a frozen-hydrated p(DTE−PEG) film after immersion of 12 months in water at 20 °C. Pixel size = 15 nm. Numbers on gray scales correspond to weight fraction. Images were smoothed with a 2 × 2 window. The arrow in (a) points to an ice crystal. Line profiles across the features inside the boxes are shown in Figure 9.

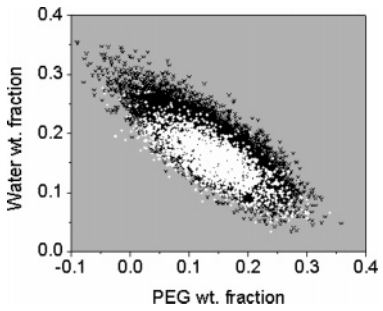

Figure 8. Water−PEG scatter diagram showing simulated noise cluster (white points) superimposed on experimental cluster (black points) generated from Figure 7.

shows the experimental cluster derived from Figure 7 (black points) over which a noise cluster (white points) centered at the composition 14.1 wt % PEG−15.6 wt % water was superimposed. The center of the noise cluster was defined as the average of the pixels within a 10 × 10 region in Figure 7 with visually uniform water and PEG distribution. Because the noise cluster no longer coincides with the experimental cluster, the scatter diagram analysis indicates that statistically significant changes have occurred to the spatial distribution of both water and PEG. More specifically, the areas with dark contrast in Figure 7b correspond to regions where PEG erosion took place. The average PEG-to-DTE ratio in these regions is below 0.10, whereas this ratio is 0.19 in the surrounding matrix.

Concomitant with the preferential loss of PEG-rich fragments, the water content in the 12 month specimen increased to 19.0 ± 1.2 wt % from the 11.8 ± 0.7 wt % of the nondegraded film. Significantly, by comparing parts a and b of Figure 7, we see that this increase occurs preferentially within the PEG-depleted domains. Specifically, from Figure 7a we obtain an average water content within the PEG-depleted regions of ∼25 wt %, and this is considerably higher than the 19.0 ± 1.2 wt % overall water content of the copolymer. To know how much water is absorbed by different regions of a bioresorbable polymer is important because the regions with higher water content should subsequently degrade at a faster rate.[36] Upon erosion,

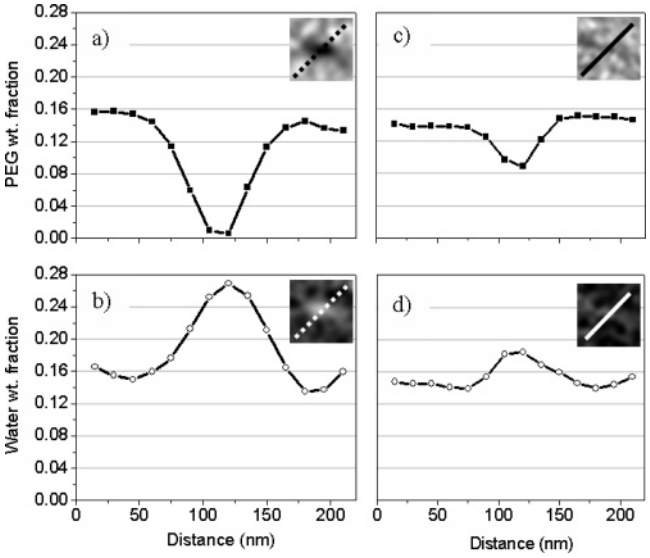

Figure 9. (a) Line profile across the circular PEG-depleted region inside of the dotted box in Figure 7b. (b) Line profile across the circular water-enriched region inside of the dotted box in Figure 7a. (c) Line profile across the elongated PEG-depleted region inside of the solid box in Figure 7b. (d) Line profile across the elongated water-enriched region inside of the solid box in Figure 7a.

such regions would subsequently accelerate local morphological changes relative to regions where the water content is lower. We observe in the middle of Figure 7a a very large water-rich feature (white arrow) but no corresponding PEG-depleted region in Figure 7b. This feature is a thin ice crystal on the specimen most likely deposited during transfer of the specimen to the microscope. Observation of this artifact and its effect on the PEG and water maps reinforces the fact that the contrast in these maps is exclusively compositional and not modulated by variations in film thickness.

A question that naturally arises concerns what possible mechanism could be at play during the erosion of the p(DTE−PEG) copolymer. After 5 months of immersion in water, no erosion is observed both by HAADF STEM imaging and compositional mapping. In agreement with previous work on bulk erosion,[7,12,16] this result indicates that water-soluble fragments produced by degradation are initially unable to diffuse through the undegraded polymer matrix and cause erosion. According to Göpferich's percolation model,[12] erosion relies on the formation of a percolated microstructure constituted by water-soluble degradation products. Because no erosion takes place in the p(DTE−PEG) system during the first 5 months of immersion in water, we conclude that a percolated microstructure has not fully formed during the 5 months. After 12 months of immersion, however, PEG-rich fragments preferentially erode from the copolymer film, suggesting that interconnected high diffusivity paths have formed.

The compositional images in Figure 7 provide direct evidence that a percolated microstructure exists in the specimen immersed in water for 12 months. The PEG map in Figure 7b shows circular as well as elongated PEG-depleted regions. These regions constitute parts of the interconnected path from which PEG-rich fragments have eroded. Compositional line profiles across a circular and an elongated PEG-depleted region are shown in Figure 9. At its center, the PEG composition of the circular structure is almost 0 wt %. The PEG composition of the elongated structure is higher (∼10 wt %) but still less than that of the surrounding matrix (∼15 wt %). We can understand these observations if we consider that the PEG-depleted features

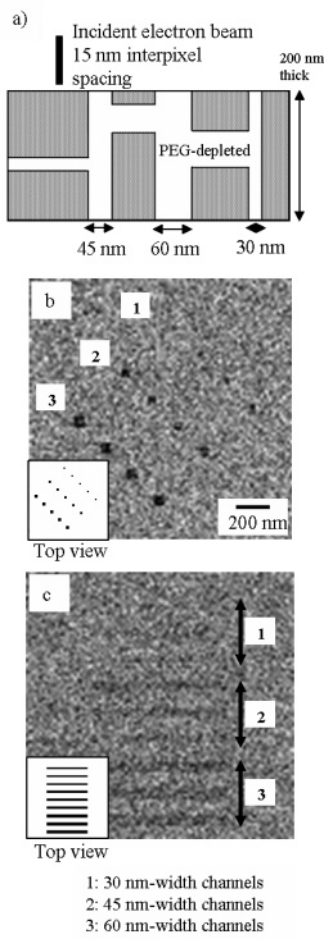

Figure 10. (a) Schematics of the cross-sectional view of a p(DTE−PEG) TEM specimen (200 nm thick) with PEG-eroded channels (30−60 nm width) vertically and horizontally aligned relative to the specimen plane. The composition of the matrix and of the channels is 15 wt % and 0% PEG, respectively. (b) Vertically aligned PEG-depleted channels (30−60 nm width) appear in a PEG map as circular structures and with high contrast. (c) Horizontally aligned PEG-depleted channels (30−60 nm width) appear in a PEG map as elongated structures and with weak contrast.

in Figure 7 correspond to channels that are oriented in all possible directions within the TEM specimen. These channels presumably form when sufficient degradation of the DTE-rich matrix has occurred so that water-soluble PEG-rich oligomers are able to diffuse out to the surface. The spectroscopic contrast we observe at the 12 month time point can vary simply because the projected specimen composition will be different for channels oriented perpendicular to the specimen plane than it will be for channels lying within the plane.

The variations in image contrast can be simulated. For example, Figure 10a schematically shows in cross section a TEM specimen 200 nm thick with channels (30−60 nm width) horizontally and vertically aligned relative to the TEM specimen plane. The compositions of the matrix and of the channels were assumed to be 15 and 0 wt % PEG, respectively, and their water compositions were ∼15 and 25 wt %, respectively. To simulate the experimental images, we assumed that an incident electron beam (15 nm in diameter) was scanned over this hypothetical specimen at a dose of 600 e/nm^2 equal to that used to generate the maps in Figure 7. Figure 10b shows how vertically aligned PEG-depleted channels would appear in projection in a PEG map when noise is included in the simulation following the protocols used to define the noise cluster in the scatter diagram

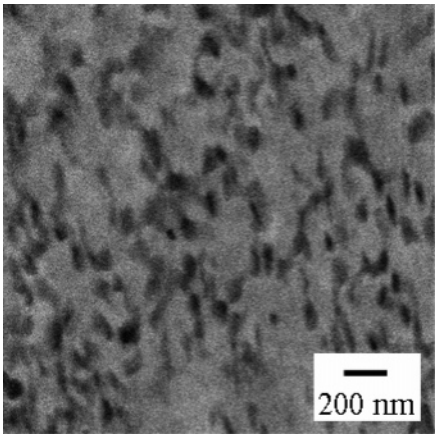

Figure 11. HAADF STEM image of a frozen-hydrated p(DTE−PEG) film after immersion of 12 months in water at 20 °C + 2 weeks at 37 °C.

(Figure 5). Namely, vertically aligned PEG-depleted regions are observed with relatively high contrast. On the other hand, horizontally aligned PEG-depleted channels appear with much weaker contrast (Figure 10c) since in projection their composition is averaged with that of the matrix above and below the channel. In the experimental PEG map (Figure 7b), we conclude that the circular high-contrast PEG-eroded regions originate from PEG-depleted channels roughly vertically aligned relative to the TEM specimen plane because only a vertical channel in projection can give rise to a feature with ∼0 wt % PEG from a ∼200 nm thick specimen. The weak-contrast PEG-depleted elongated structures in Figure 7b, on the other hand, originate from PEG-depleted channels roughly horizontally aligned. Figure 10c reveals that 30 nm width horizontally aligned channels are at the threshold of visibility. Thus, PEG-eroded channels approximately 2−3 pixels wide (30−45 nm width) potentially present in the 12 month specimen would be virtually undetectable due to the low compositional contrast that they generate and the intrinsic noise associated with these experiments. Furthermore, PEG-eroded channels that are small and too close together cannot be directly observed in a PEG map since in projection they appear superimposed and indistinguishable from each other. Microtoming thinner TEM specimens and pushing further the limits of spatial resolution of the EELS technique would potentially allow us to observe PEG-depleted regions such as the ones in Figure 7b with characteristic length scales finer than ∼30−45 nm.

The morphological changes observed after 12 months of immersion in water at 20 °C represent an early stage of erosion. We found that the extent of percolation increased with continued degradation. To accelerate degradation, we placed a copolymer film exposed to water for 12 months at 20 °C for an additional 2 weeks in water at 37 °C. At this higher temperature, hydrolysis rates and diffusion rates are both enhanced as indicated by a substantially higher fraction of eroded areas with a greater degree of interconnectedness (Figure 11). Cryo-ultramicrotoming multiphase materials such as these highly hydrated copolymers with heterogeneous mechanical properties is a practical challenge, and local variations in microtomed specimen thickness precluded us from performing quantitative spectroscopy imaging on these 12 month + 2 week specimens. However, relative-thickness measurements with EELS in the STEM[23] provide evidence that at this later time point DTE-rich fragments have left the specimen in addition to the PEG-rich fragments which are able to leave at earlier time points.

4. Conclusions

We have exploited the combination of spatial resolution and spectral sensitivity afforded by EELS in the STEM to quantify the nanoscale evolution of morphology in a bioresorbable copolymer. By further combining this approach with cryo-microscopy techniques, we were able to measure the spatial distribution not only of the two polymer species in the copolymer but also of the water. This new imaging method has enabled us to study the dynamic hydrated morphology both more quantitatively and at length scales much finer than other characterization methods previously used to study erosion. Compositional mapping from a p(DTE−PEG) copolymer film immersed in water for 12 months revealed PEG-depleted regions with characteristic length scales of 50−100 nm. These regions correspond to a percolated network of high-diffusivity channels through which PEG-rich fragments had eroded. The PEG-depleted regions are enriched in water, consistent with the idea that erosion creates free volume that can be occupied by in-diffused water. Our observations at the nanoscale reinforce the concept introduced by Göpferich that highlights the central importance of percolation in bulk-eroding systems.

Acknowledgment. This research project has been supported through RESBIO−The National Resource for Polymeric Biomaterials (NIH Grant EB001046) and uses instrumentation supported by the National Science Foundation and by DOD DURIP Grants DAD19-99-1-0110 and W911NF-04-1-0136.

References and Notes

(1) Xue, L.; Greisler, H. P. *J. Vasc. Surg.* **2003**, *37*, 472−480.
(2) Panyam, J.; Labhasetwar, V. *Adv. Drug Delivery Rev.* **2003**, *55*, 329−347.
(3) Langer, R.; Vacanti, J. *Science* **1995**, *260*, 920−926.
(4) Kumar, N.; Ravikumar, M. N.; Domb, A. J. *Adv. Drug Delivery Rev.* **2001**, *53*, 23−44.
(5) Göpferich, A. *Biomaterials* **1996**, *17*, 103−114.
(6) Göpferich, A.; Langer, R. *J. Polym. Sci., Part A: Polym. Chem.* **1993**, *31*, 2445−2458.
(7) Burkersroda, F.; Gref, R.; Göpferich, A. *Biomaterials* **1997**, *18*, 1599−1607.
(8) Shakesheff, K. M.; Davies, M. C.; Roberts, C. J.; Tendler, S. J.; Shard, A. G.; Domb, A. *Langmuir* **1994**, *10*, 4417−4419.
(9) Hurrell, S.; Cameron, R. E. *J. Mater. Sci.: Mater. Med.* **2001**, *12*, 811−816.
(10) Batycky, R. P.; Hanes, J.; Langer, R.; Edwards, D. *J. Pharm. Sci.* **1997**, *86*, 1464−1477.
(11) Göpferich, A.; Langer, R. *Macromolecules* **1993**, *26*, 4105−4112.
(12) Göpferich, A. *Macromolecules* **1997**, *30*, 2598−2604.
(13) Lyu, S.; Sparer, R.; Untereker, D. *J. Polym. Sci., Part B: Polym. Phys.* **2005**, *43*, 383−397.
(14) Kipper, M. J.; Narasimhan, B. *Macromolecules* **2005**, *38*, 1989−1999.
(15) Burkersroda, F. v.; Schedl, L.; Göpferich, A. *Biomaterials* **2002**, *23*, 4221−4231.
(16) Asano, M.; Fukuzaki, H.; Yoshida, M.; Kumakura, M.; Mashimo, T.; Yuasa, H.; Imai, K.; Yamanaka, H. *Drug Des. Delivery* **1990**, *5*, 301−320.
(17) Li, S. M.; Vert, M. *J. Biomater. Sci., Polym. Ed.* **1996**, *7*, 817−827.
(18) Göpferich, A.; Tessmar, J. *Adv. Drug Delivery Rev.* **2002**, *54*, 911−931.
(19) Yu, C.; Kohn, J. *Biomaterials* **1999**, *20*, 253−264.
(20) Shakesheff, K. M.; Chen, X.; Davies, M. C.; Domb, A.; Roberts, C. J.; Tendler, S. J. B.; Williams, P. M. *Langmuir* **1995**, *11*, 3921−3927.
(21) Kipper, M.; Seifert, S.; Thiyagarajan, P.; Narasimhan, B. *Polymer* **2004**, *45*, 3329−3340.
(22) Libera, M.; Disko, M. Electron Energy-Loss Spectroscopy of Polymers. In *Transmission Electron Energy Loss Spectroscopy in Materials Science and the EELS ATLAS*, 2nd ed.; Ahn, C., Ed.; Wiley-VCH Verlag Gmbh & Co. KGaA: Weinheim, 2004.
(23) Egerton, R. F. *Electron Energy-Loss Spectroscopy in the Electron Microscope*, 2nd ed.; Plenum Press: New York, 1996.

(24) Batson, P. E.; Dellby, N.; Krivanek, O. L. *Nature (London)* **2002**, *418*, 617−620.
(25) Sousa, A.; Aitouchen, A.; Libera, M. *Ultramicroscopy* **2006**, *106*, 130−145.
(26) Sun, S.; Shi, S.; Hunt, J.; Leapman, R. *J. Microsc.* **1995**, *177*, 18−30.
(27) Aitouchen, A.; Shi, S.; Libera, M.; Misra, M. *Microsc. Microanal.* **2002**, *8* (Suppl. 2), 284−285.
(28) Terryn, C.; Michel, J.; Thomas, X.; Laurent-Maquin, D.; Balossier, G. *Eur. Biophys. J.* **2004**, *33*, 321−327.
(29) Bourke, S. L.; Kohn, J. *Adv. Drug Delivery Rev.* **2003**, *55*, 447−466.
(30) Tangpasuthadol, V.; Pendharkar, S. M.; Peterson, R. C.; Kohn, J. *Biomaterials* **2000**, *21*, 2379−2387.
(31) Leapman, R.; Sun, S. *Ultramicroscopy* **1995**, *59*, 71−79.
(32) Sun, S.; Shi, S.; Leapman, R. *Ultramicroscopy* **1993**, *50*, 127−139.
(33) Sawyer, L. C.; Grubb, D. *Polymer Microscopy*, 2nd ed.; Chapman and Hall: London, 1996.
(34) Chou, T. M.; Prayoonthong, P.; Aitouchen, A.; Libera, M. *Polymer* **2002**, *43*, 2085−2088.
(35) Thakur, R.; Sousa, A.; Michniak, M. L. B.; Kohn, J. Proc.IEEE 31st Annu. Northeast, 2005; IEEE: 2005; pp 197−199.
(36) Shah, S. S.; Zhu, K. J.; Pitt, C. G. *J. Biomater. Sci., Polym. Ed.* **1994**, *5*, 421−431.

MA061286G